The Astrophysical Journal, 1012:219 (12pp), 2026 December 1 https://doi.org/10.3847/1538-4357/aeba7c
© 2026. The Author(s). Published by the American Astronomical Society.
OPEN ACCESS

Abiotic Formation of Oxalic Acid (HOOCCOOH) in Interstellar Analog Ices of Carbon Dioxide and Methanol

Jia Wang[1,2,4], Musahid Ahmed[3], and Ralf I. Kaiser[1,2]
[1] W. M. Keck Research Laboratory in Astrochemistry, University of Hawaii at Manoa, Honolulu, Hawaii 96822, USA; ralfk@hawaii.edu
[2] Department of Chemistry, University of Hawaii at Manoa, Honolulu, Hawaii 96822, USA
[3] Chemical Sciences Division, Lawrence Berkeley National Laboratory, Berkeley, California 94720, USA
Received 2026 July 30; revised 2026 October 22; accepted 2026 October 26; published 2026 November 25

Abstract

Dicarboxylic acids have been identified in carbonaceous chondrites and in pristine samples returned from carbonaceous asteroids such as Ryugu, supporting their extraterrestrial origin and possible exogenous delivery to the early Earth, with potential implications for the molecular origins of life. However, their formation mechanisms under astrophysical conditions remain poorly understood. Here, we present the first laboratory experiments demonstrating the formation of oxalic acid (HOOCCOOH)—the simplest dicarboxylic acid—in interstellar analog ices composed of carbon dioxide (CO_2) and methanol (CH_3OH). The low-temperature ice mixtures were irradiated with energetic electrons, simulating secondary electrons generated during the interaction of galactic cosmic rays (GCRs) with interstellar ices. The deposited irradiation dose corresponds to $(7 \pm 1) \times 10^6$ yr of GCR exposure in a cold molecular cloud. Utilizing vacuum ultraviolet photoionization reflectron time-of-flight mass spectrometry (PI-ReToF-MS) together with isotopic substitution experiments, oxalic acid was isomer-selectively identified in the gas phase during temperature-programmed desorption based on its adiabatic ionization energy and dissociative photoionization fragmentation pattern. These findings suggest that oxalic acid represents a suitable target for future astronomical searches. The formation of oxalic acid is proposed to proceed via suprathermal hydrogen-atom addition to carbon dioxide, yielding hydroxycarbonyl radicals, followed by their barrierless radical–radical recombination. Our results reveal a feasible formation pathway for oxalic acid in carbon dioxide-bearing interstellar ices through GCR-driven nonequilibrium chemistry, providing useful insights into the abiotic synthesis and astrochemical evolution of dicarboxylic acids in extraterrestrial environments.

Unified Astronomy Thesaurus concepts: Laboratory astrophysics (2004); Astrochemistry (75); Mass spectrometry (2094); Complex organic molecules (2256); Interstellar molecules (849)

1. Introduction

Since the first detection of oxalic acid (HOOCCOOH) in extracts of the Murchison meteorite more than half a century ago (J. G. Lawless et al. 1974), dicarboxylic acids—organic compounds containing two carboxyl groups (−COOH)—have attracted considerable attention across laboratory astrophysics (C. K. Materese et al. 2013; C. K. Materese et al. 2014; B. M. McMurtry et al. 2016a, 2016b), astrochemistry (L. Remusat et al. 2005; Y. Takano et al. 2024), physical chemistry (R. Komorek et al. 2018), and prebiotic chemistry (N. R. Lerner & G. W. Cooper 2005; N. Mukherjee & U. K. Ghorai 2025). This interest is mainly due to their roles in the abiotic synthesis of clay minerals and molecular growth toward biorelevant molecules (G. Cooper et al. 2011; D. Schumann et al. 2012; M. R. Marín-Yaseli et al. 2016; N. Mukherjee & U. K. Ghorai 2025). Although no dicarboxylic acid has yet been detected in the interstellar medium (ISM), more than 50 oxygen-containing complex organic molecules (COMs)—defined as carbon-containing molecules comprising six or more atoms (E. Herbst & E. F. V. Dishoeck 2009)—have been (tentatively) identified in the ISM (Figure 1), including alcohols, aldehydes, ketones, carboxylic acids, amides, esters, and ethers and accounting for approximately 14% of the 367 known interstellar molecules.[5] Notably, the cis–trans conformer of carbonic acid (HOCOOH; Figure 1) was recently detected toward the Galactic center molecular cloud G+0.693–0.027 using the Yebes 40 m and IRAM 30 m telescopes (M. Sanz-Novo et al. 2023), demonstrating that highly oxygenated acids containing three oxygen atoms can form and survive under interstellar conditions and raising the possibility that dicarboxylic acids may also be synthesized and persist in such environments (V. M. Rivilla et al. 2026).

In contrast, a variety of dicarboxylic acids ranging from the C_2 species oxalic acid to the C_9 compounds such as azelaic acid ($HOOC(CH_2)_7COOH$) have been identified in carbonaceous chondrites (E. T. Peltzer et al. 1984; A. Shimoyama & R. Shigematsu 1994), with oxalic acid reaching a concentration of 9.2 $\mu g\ g^{-1}$ in the Murchison meteorite (E. T. Peltzer et al. 1984). More recently, analyses of pristine samples returned from the carbonaceous asteroid Ryugu by JAXA's Hayabusa2 mission revealed multiple dicarboxylic acids including oxalic acid, malonic acid ($HOOCCH_2COOH$), maleic acid ($HOOC(CH)_2COOH$), succinic acid ($HOOC(CH_2)_2COOH$), glutaric acid ($HOOC(CH_2)_3COOH$), and adipic acid ($HOOC(CH_2)_4COOH$), with oxalic acid present at a concentration of 1.1 $\mu g\ g^{-1}$ (Y. Takano et al. 2024). The occurrence of dicarboxylic acids in both meteorites

[4] Present address: College of Engineering Physics, Shenzhen Technology University, Shenzhen 518118, People's Republic of China.

[5] D. E. Woon, The Astrochymist, http://www.astrochymist.org (accessed July 16, 2026).

Original content from this work may be used under the terms of the Creative Commons Attribution 4.0 licence. Any further distribution of this work must maintain attribution to the author(s) and the title of the work, journal citation and DOI.

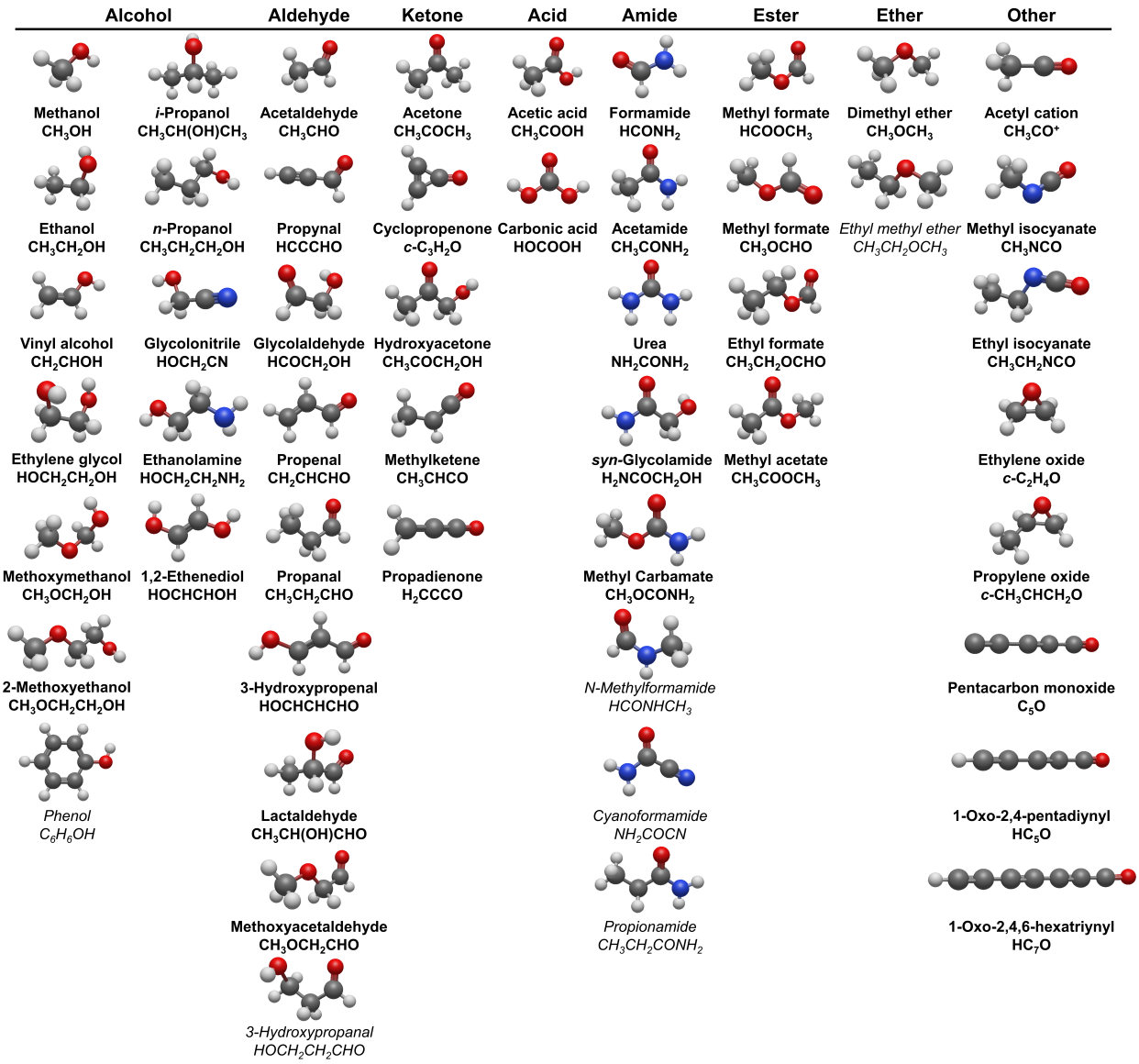

Figure 1. Oxygen-containing complex organic molecules (COMs) identified in extraterrestrial environments in the gas phase. Molecules in italics represent tentative identifications. Atoms are color coded: black for carbon, gray for hydrogen, red for oxygen, and blue for nitrogen.

and pristine asteroid samples supports their extraterrestrial origin and subsequent exogenous delivery to the early Earth. Nevertheless, the fundamental reaction pathways for their abiotic formation under astrophysically relevant conditions remain poorly understood, particularly for oxalic acid, the simplest dicarboxylic acid.

Laboratory simulation experiments have demonstrated the formation of oxalic acid in ultraviolet (UV)-irradiated pyrimidine-containing ice mixtures and its detection via gas chromatography–mass spectrometry (GC–MS) analysis of the resulting refractory residues (C. K. Materese et al. 2013; C. K. Materese et al. 2014; M. Nuevo & S. A. Sandford 2014). These ice mixtures include methanol (CH_3OH)–pyrimidine ($C_4H_4N_2$), water (H_2O)–methanol–pyrimidine, methane (CH_4)–pyrimidine, and water–methane–pyrimidine ices (C. K. Materese et al. 2013), as well as water–methanol–ammonia (NH_3)–pyrimidine and water–methanol–methane–ammonia–pyrimidine ices (M. Nuevo & S. A. Sandford 2014). Oxalic acid was identified in refractory residues produced by UV irradiation of nitrogen (N_2)–methane–carbon monoxide (CO) ices (C. K. Materese et al. 2014). More recently, oxalic acid was also tentatively assigned during the warm-up of UV-processed acetic acid (CH_3COOH)–water ices (C. d. B. Olivares et al. 2024). Irradiation of carbon dioxide (CO_2)-containing hydrocarbon ices with energetic electrons suggested oxalic acid may form through the barrierless recombination of two hydroxycarbonyl (HOCO) radicals, although oxalic acid itself was not conclusively identified (Y. S. Kim & R. I. Kaiser 2010). Similarly, GC–MS signals tentatively assigned to oxalic acid were observed in residues produced by irradiating N_2–CH_4–CO ices with energetic electrons; however, this assignment could not be validated through isotopic substitution experiments and was further complicated by the presence of corresponding signals in blank experiments (C. K. Materese et al. 2015). Thus, oxalic acid has been identified primarily through an offline GC–MS analysis of refractory residues obtained after warming processed ices; however, its direct isomer-selective identification in the gas

phase upon sublimation from interstellar analog ices has remained elusive.

Here, we present the first laboratory experiments demonstrating the formation of oxalic acid (HOOCCOOH) in model interstellar ices composed of carbon dioxide (CO_2) and methanol (CH_3OH) exposed to galactic cosmic ray (GCR) proxies in the form of energetic electrons. The low-temperature (5 K) ice mixtures were irradiated with energetic electrons, simulating the secondary electrons generated by GCRs in interstellar ices (R. Kaiser & K. Roessler 1997; B. C. Ferrari et al. 2021; J. Wang et al. 2024c). The irradiation dose corresponds to $(7 \pm 1) \times 10^6$ yr of GCR exposure in interstellar ices, representative of an evolved stage of a cold molecular cloud (A. G. Yeghikyan 2011). Utilizing vacuum ultraviolet (VUV) photoionization reflectron time-of-flight mass spectrometry (PI-ReToF-MS) in conjunction with isotopic substitution experiments, oxalic acid was isomer-selectively identified in the gas phase during temperature-programmed desorption (TPD) based on its experimentally measured adiabatic ionization energy (IE) and characteristic dissociative photoionization fragmentation patterns.

Carbon dioxide is one of the most abundant constituents of interstellar ices and has been detected toward background stars such as Elias 16 (D. C. B. Whittet et al. 1998), NIR38, and J110621 (M. K. McClure et al. 2023), toward young stellar objects (YSOs) (K. M. Pontoppidan et al. 2008), and in protoplanetary disks such as HH 48 NE (J. A. Sturm et al. 2023), with abundances reaching up to 40% relative to water toward AFGL 989 (E. L. Gibb et al. 2004). Methanol has been detected on interstellar grains toward low-mass protostars such as IRAS 16293−2422 (B. Parise et al. 2002; S. Cazaux et al. 2003) as well as toward high-mass protostars; notably, it is the second most abundant ice species toward the high-mass protostars such as RAFGL7009S and W33A, reaching abundances of up to 30% relative to water (E. Dartois et al. 1999). Therefore, carbon dioxide–methanol ice serves as a suitable model of interstellar ice for investigating the formation of oxygen-containing COMs such as oxalic acid. Our results reveal that oxalic acid can be synthesized in carbon dioxide- and methanol-rich interstellar ices via GCR-induced nonequilibrium chemistry, suggesting that the previously astronomically undetected oxalic acid represents a promising target for future astronomical search via telescopes such as the Atacama Large Millimeter/submillimeter Array (ALMA) and the James Webb Space Telescope (JWST). These findings advance our fundamental understanding of the formation of oxalic acid in carbon dioxide-containing interstellar ices through GCR-driven processes, providing useful insights into the abiotic synthesis and astrochemical evolution of dicarboxylic acids in deep space.

2. Experimental Section

The experiments were carried out in an ultrahigh vacuum chamber maintained at a few 10^{-11} Torr using magnetically levitated turbomolecular pumps backed by a dry scroll pump (B. M. Jones & R. I. Kaiser 2013; R. I. Kaiser et al. 2014). A two-stage closed-cycle helium cryostat cooled a polished silver substrate to 5 K, while the cryostat–substrate assembly could be rotated within the horizontal plane and translated vertically. The experimental procedures have been described previously (J. H. Marks et al. 2023a). Briefly, the ice mixtures were prepared by codepositing carbon dioxide (CO_2, Airgas, 99.999%; $^{13}CO_2$, Sigma-Aldrich, 99% atom ^{13}C) and methanol vapor (CH_3OH, Fisher Scientific, $>$ 99.8%; $^{13}CH_3OH$, Sigma-Aldrich, 99.9%, CD_3OD, Sigma-Aldrich, $\geqslant$ 99.8 atom % D) through separate glass capillary arrays directed toward the silver substrate maintained at 5.0 ± 0.2 K. Although this temperature is slightly below those typical of cold molecular clouds, reactive intermediates can remain stabilized at 5 K, thereby facilitating a clearer mechanistic interpretation of the experimental results (J. Wang et al. 2024c). During deposition, the partial pressures of methanol and carbon dioxide were each maintained at 2×10^{-8} Torr, while the ice thickness was monitored by laser interferometry (A. M. Turner et al. 2015) and determined to be 750 ± 50 nm using an average refractive index of 1.28 ± 0.02, derived from values of 1.27 ± 0.02 for carbon dioxide at 20–25 K (M. Bouilloud et al. 2015) and 1.296 for methanol at 15 K (R. L. Hudson et al. 2020). Following deposition, Fourier transform infrared (FTIR) spectra were recorded over the range 6000–500 cm^{-1} using a Nicolet 6700 spectrometer (Thermo Electron). The relative concentrations of CO_2 and CH_3OH in the ices were determined to be (0.9 ± 0.33):1 from the integrated infrared absorptions and their corresponding band strengths (J. H. Marks et al. 2023a).

After deposition, the ices were irradiated with 5 keV electrons at a current of 50 nA for 30 minutes over an area of 160 mm^2 at an incidence angle of 70°. These energetic electrons simulate secondary electrons generated along the tracks of GCRs penetrating interstellar ices (A. Bergantini et al. 2017; A. Bergantini et al. 2018a, 2018b). The irradiation doses were calculated to be 3.2 ± 0.3 eV $molecule^{-1}$ for carbon dioxide and 2.3 ± 0.2 eV $molecule^{-1}$ for methanol (J. H. Marks et al. 2023a), corresponding to a GCR exposure time of $(7 \pm 1) \times 10^6$ yr under conditions representative of an evolved stage of a cold molecular cloud (A. G. Yeghikyan 2011). Monte Carlo simulations using the CASINO 2.42 software suite (D. Drouin et al. 2007) yielded an average electron penetration depth of 320 ± 30 nm for the CO_2–CH_3OH ices (J. H. Marks et al. 2023a), substantially smaller than the total ice thickness of 750 ± 50 nm, thus minimizing interactions of the energetic electrons with the silver substrate. FTIR spectra were recorded during and after irradiation to monitor chemical changes in the ices. After irradiation, the ices were heated from 5 to 320 K at a rate of 0.5 K min^{-1} under TPD conditions. During TPD, pulsed VUV light operating at 30 Hz was directed approximately 2 mm above the ice surface to photoionize subliming molecules. VUV photons at 11.10, 10.56, and 9.93 eV were generated through resonant four-wave mixing ($\omega_{VUV} = 2\omega_1 \pm \omega_2$) using combinations of dye lasers (Sirah Lasertechnik, Cobra-Stretch) and Nd:YAG lasers (Spectra-Physics, Quanta Ray PRO 270-30). To generate 11.10 eV photons, sum-frequency generation ($2\omega_1 + \omega_2$) employed 249.6 nm (ω_1) with two-photon resonance of xenon together with 1064 nm (ω_2). Photons at 10.56 and 9.93 eV were generated by difference-frequency mixing ($2\omega_1 - \omega_2$) in pulsed krypton gas using 202.316 nm (ω_1) together with a second dye laser operating at 730.836 or 532.929 nm (ω_2), respectively (J. H. Marks et al. 2023a). The generated VUV beam was separated from the fundamental laser beams using an off-axis lithium fluoride biconvex lens and directed into the photoionization region, where the resulting ions were mass analyzed with a reflectron time-of-flight mass spectrometer (ReToF-MS; Jordan TOF Products) and detected using a dual microchannel plate (MCP) detector. The MCP signal was amplified,

discriminated, and further amplified to an amplitude of 4 V, and recorded using a multichannel scaler (FAST ComTec, MCS6A) with a temporal resolution of 3.2 ns (J. H. Marks et al. 2023a). Each mass spectrum was acquired at 30 Hz and accumulated over 2 minutes (3600 sweeps) throughout the TPD phase. A blank (control) experiment using unirradiated CO_2-CH_3OH ice was also conducted using 11.10 eV photoionization.

3. Results and Discussion

FTIR spectra of carbon dioxide–methanol ices recorded before and after irradiation at 5 K have been described previously (J. H. Marks et al. 2023a). Electron irradiation produced several new absorption features, including the CO stretching mode of carbon monoxide (CO) at 2136 cm^{-1} (S. Maity et al. 2015), the C=O stretching mode of formaldehyde (H_2CO) at 1722 cm^{-1} (ν_2) (T. Butscher et al. 2016), and the asymmetric deformation mode of methane (CH_4) at 1292 cm^{-1} (ν_4) (M. Bouilloud et al. 2015; J. Wang et al. 2025b) (Figure A1). Additional absorptions at 1773 and 1653 cm^{-1} indicate the formation of one or more carbonyl (C=O)-bearing species and hydrogen-bonded carboxylic acids, respectively (G. Socrates 2004). Previous measurements revealed that oxalic acid ice exhibits absorption features at 1280 and 1770 cm^{-1} assigned to the OH bending (δ_{COH}) mode and C=O stretching mode, respectively (J. De Villepin et al. 1982; H. Yan & L. T. Chu 2008); therefore, the observed absorptions at 1292 and 1773 cm^{-1} may contain contributions from oxalic acid. Additionally, the O–H stretching band of oxalic acid is expected to overlap with the broad and intense O–H stretching band of methanol (J. De Villepin et al. 1982). A weak absorption at 1845 cm^{-1} can be assigned to the trans-hydroxycarbonyl radical (ν_2) (D. E. Milligan & M. E. Jacox 1971) and the same feature is also observed in an additional higher-dose (100 nA, 60 minutes) experiment (Figure A1). Although infrared results indicate the formation of carbonyl-bearing species and carboxylic acids, FTIR spectroscopy alone does not permit the unambiguous identification of individual complex carboxylic acids formed in the ices, highlighting the need for a more sensitive, isomer-selective technique to identify the $C_2H_2O_4$ isomers.

PI-ReToF-MS was employed to identify oxalic acid isomer-selectively through measurement of distinct adiabatic IEs and desorption temperature profiles (A. M. Turner & R. I. Kaiser 2020; J. Wang et al. 2025a). VUV photons at 11.10, 10.56, and 9.93 eV were used to photoionize products subliming from the processed ices during TPD. Focusing on $C_2H_2O_4$ isomers, the TPD profile of the ion signal at a mass-to-charge (m/z) of 90 from the irradiated CO_2-CH_3OH ice revealed an intense sublimation event peaking near 234 K (Peak I), followed by a broad sublimation event extending to 307 K (Figure 2(a)). The minor sublimation event near 144 K is attributed to cosublimation with methanol. A blank experiment using unirradiated CO_2–CH_3OH ice was conducted under otherwise identical conditions; no ion signal of $m/z = 90$ was detected, confirming that the observed sublimation events originated from electron-induced processing of the ice mixture. To confirm the molecular formula associated with $m/z = 90$, separate irradiation experiments were conducted using fully deuterated CO_2–CD_3OD ice and fully ^{13}C-labeled $^{13}CO_2$–$^{13}CH_3OH$ ice. The TPD profile of $m/z = 92$ from the irradiated CO_2–CD_3OD ice matched well with that of $m/z = 90$ from the irradiated CO_2–CH_3OH ice (Figure 2(b)), demonstrating the incorporation of two hydrogen atoms into the carrier of $m/z = 90$. Likewise, the TPD profile of $m/z = 90$ in the irradiated CO_2–CH_3OH ice shifted to $m/z = 92$ in the irradiated $^{13}CO_2$–$^{13}CH_3OH$ ice, confirming the presence of two carbon atoms (Figure 2(c)). Therefore, these isotopic shifts establish that the sublimation events of $m/z = 90$ from the irradiated CO_2–CH_3OH ice arise from species with the molecular formula $C_2H_2O_4$.

As mentioned above, the TPD profile of $m/z = 90$ ($C_2H_2O_4^+$) from the irradiated CO_2–CH_3OH ice exhibits Peak I at 234 K and a broad sublimation event extending to 307 K. At 11.10 eV, oxalic acid (IE = 10.9 ± 0.1 eV) (R. Komorek et al. 2018) can be photoionized; therefore, these sublimation events can be associated with oxalic acid and/or other $C_2H_2O_4$ isomers. Lowering the photon energy to 10.56 eV, at which oxalic acid cannot be photoionized, results in the disappearance of Peak I, whereas the broad sublimation event remains (Figure 2(a)), indicating that Peak I could be assigned to oxalic acid. Notably, the peak desorption temperature of Peak I (234 K) agrees with previous measurements of oxalic acid desorption from a copper surface, which revealed a peak sublimation temperature near 241 K (H. Yan & L. T. Chu 2008). Upon further reducing the photon energy to 9.93 eV, the remaining broad sublimation event disappears (Figure 2(a)). Therefore, this broad sublimation event can be attributed to one or more additional $C_2H_2O_4$ isomer(s) with IEs lying between 9.93 and 10.56 eV. Possible $C_2H_2O_4$ candidates linked to this broad sublimation event may be formic carbonic anhydride (HC(O)OCOOH), diformyl peroxide (HC(O)OOCHO), 2-oxoethaneperoxoic acid (HC(O)C(O)OOH), and/or dioxiranecarboxylic acid (*c*-OOCHCOOH).

A previous VUV photoionization mass spectrum of oxalic acid vapor, generated by evaporation from an aqueous solution and recorded at a photon energy of 11.10 eV (R. Komorek et al. 2018), revealed extensive fragmentation, with the fragment ion signals at $m/z = 33$, 45, 46, and 62, and a comparatively weak parent ion signal at $m/z = 90$ (Figure A2). Photoionization with excess energy above the ionization threshold can lead to intramolecular vibrational energy redistribution (J. Wang et al. 2023b; J. Wang et al. 2024b), whereas charge delocalization within the radical cation can stabilize the resulting fragment ions through hyperconjugation (I. Fernández & G. Frenking 2007; M. Xie et al. 2015). The fragment ions at $m/z = 33$ (HO_2^+), 45 (CHO_2^+), 46 ($CH_2O_2^+$), and 62 ($CH_2O_3^+$) correspond to losses of C_2HO_2, CHO_2, CO_2, and CO, respectively, from the oxalic acid radical cation ($C_2H_2O_4^+$). Importantly, Peak I of the TPD profile of $m/z = 90$ ($C_2H_2O_4^+$) is also reproduced in the TPD profiles of $m/z = 33$, 45, 46, and 62 from the irradiated CO_2–CH_3OH ice at 11.10 eV (Figures 3(a)–(d)). Based on the corresponding mass shifts observed in the fully deuterated CO_2–CD_3OD ice and fully ^{13}C-labeled $^{13}CO_2$–$^{13}CH_3OH$ ice (Figures 3(e)–(l)), these signals can be assigned to HO_2^+, CHO_2^+, $CH_2O_2^+$, and $CH_2O_3^+$, respectively. The coincidence of these TPD profiles with Peak I at $m/z = 90$ indicates that these ion signals originate from the dissociative photoionization of oxalic acid, thereby supporting its formation in the irradiated ice. Furthermore, when the photon energy is reduced to 10.56 eV, Peak I is absent not only for the TPD profile at $m/z = 90$ ($C_2H_2O_4^+$) but also for the TPD profiles of each of the fragment ions at $m/z = 33$, 45, 46, and 62, providing additional evidence for the identification of oxalic acid. Additionally, we

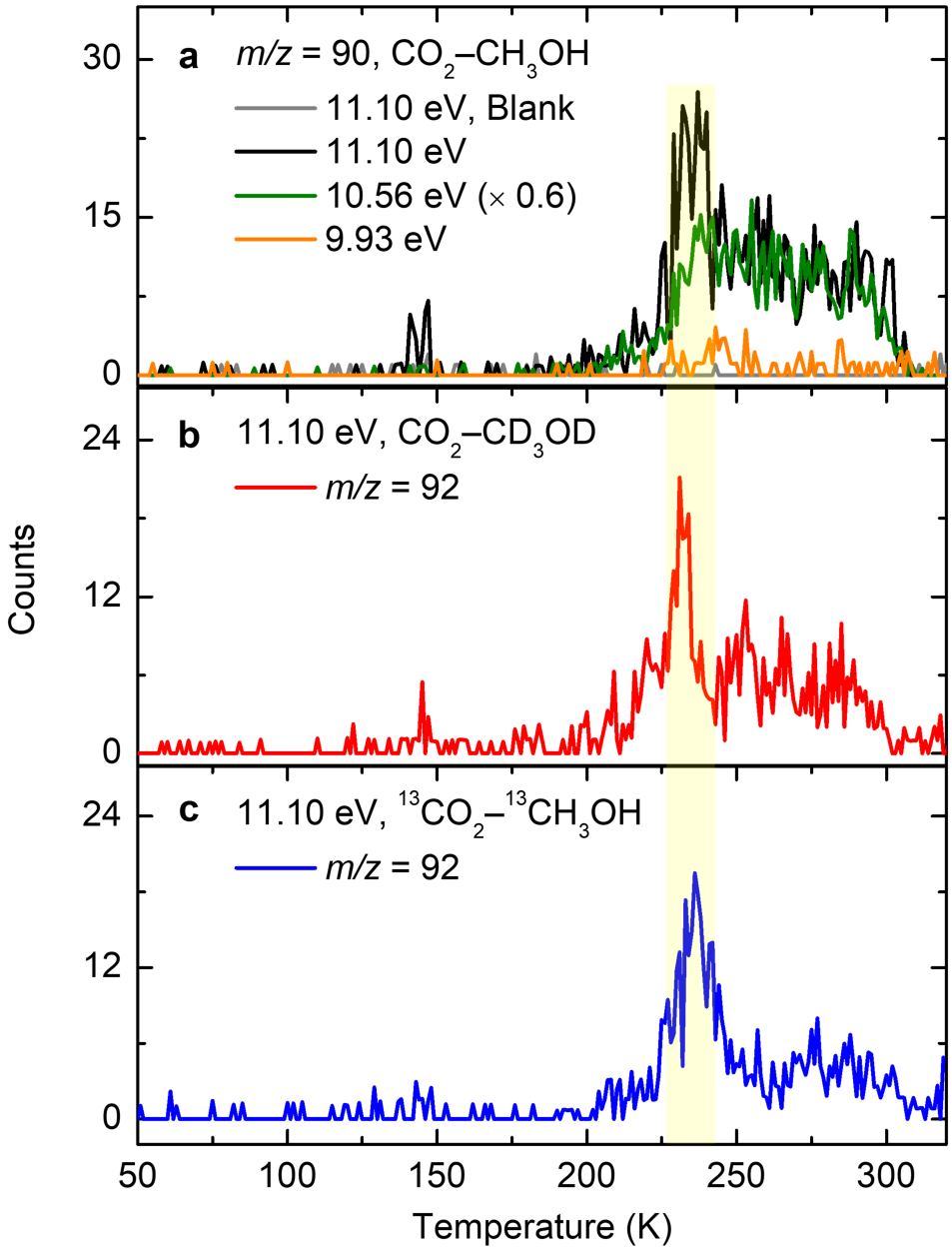

Figure 2. Ion signal recorded during temperature-programmed desorption (TPD) of carbon dioxide–methanol ice mixtures. (a) TPD profiles of $m/z = 90$ from irradiated CO_2–CH_3OH ice measured at 11.10, 10.56, and 9.93 eV, (b) $m/z = 92$ from irradiated CO_2–CD_3OD ice at 11.10 eV, and (c) $m/z = 92$ from irradiated $^{13}CO_2$–$^{13}CH_3OH$ ice at 11.10 eV. The yellow shaded regions indicate the peak sublimation temperatures of oxalic acid.

integrated the ion counts of these fragment and parent ions and plotted their intensities as a function of the mass-to-charge ratio. Figure 4 compares the resulting fragmentation pattern obtained from the irradiated CO_2–CH_3OH ice at 11.10 eV with the ReToF mass spectrum of gas-phase oxalic acid generated from an aqueous solution and recorded at the same photoionization energy (R. Komorek et al. 2018). The observed deviations in relative intensities may arise from temperature-dependent effects upon photoionization and/or from the presence of multiple oxalic acid conformers formed in our irradiated ices, which could exhibit different fragmentation behavior.

Having provided evidence for the formation of oxalic acid in irradiated carbon dioxide–methanol ices under astrophysically relevant conditions, we now focus on its potential formation mechanism. In the experiments, the ice mixtures were irradiated with energetic electrons at doses of approximately 3.2 ± 0.3 eV molecule^{-1} for carbon dioxide and 2.3 ± 0.2 eV molecule^{-1} for methanol (J. H. Marks et al. 2023a); these relatively low irradiation doses were selected to minimize secondary and consecutive reactions. The experiments were conducted at 5 K to probe low-temperature chemistry under nonequilibrium conditions, where the mobility of radicals is strongly restricted and reactive intermediates can remain trapped within the ices. First, upon interaction with energetic electrons, methanol undergoes unimolecular decomposition to yield a suprathermal hydrogen atom (H) together with the hydroxymethyl (CH_2OH) radical (reaction (1)) or the methoxy (CH_3O) radical (reaction (2)) through C–H and O–H bond cleavage, respectively. These processes have been

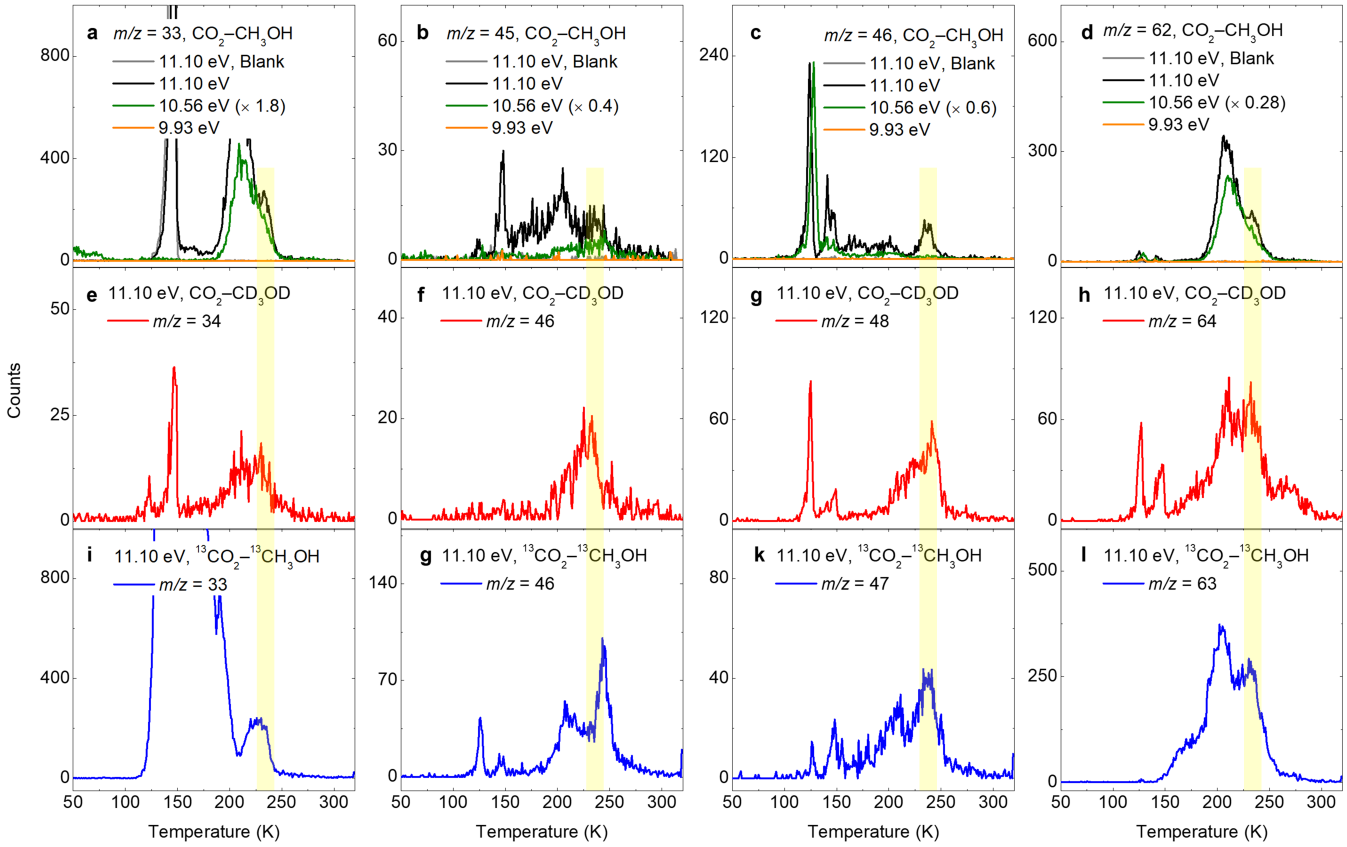

Figure 3. TPD profiles of selected mass channels corresponding to characteristic fragment ions of oxalic acid together with their isotopically substituted counterparts. TPD profiles of $m/z = 33$ (a), 45 (b), 46 (c), and 62 (d) from irradiated CO_2–CH_3OH ice measured at 11.10, 10.56, and 9.93 eV, $m/z = 34$ (e), 46 (f), 48 (g), and 64 (h) from irradiated CO_2–CD_3OD ice measured at 11.10 eV, and $m/z = 33$ (i), 46 (j), 47 (k), and 63 (l) from $^{13}CO_2$–$^{13}CH_3OH$ ice measured at 11.10 eV. The yellow shaded regions indicate the peak sublimation temperatures of oxalic acid.

demonstrated previously by laboratory simulation experiments on electron-irradiated methanol-containing ices (S. Maity et al. 2015; C. Zhu et al. 2019; J. H. Marks et al. 2023a; J. Wang et al. 2023a; J. H. Marks et al. 2024). Reactions (1) and (2) are endoergic by 395.9 ± 0.3 and 435.0 ± 0.3 kJ mol^{-1}, respectively (B. Ruscic & H. Bross 2026); the required energies can be supplied through energy deposited by the impinging electrons (R. Kaiser et al. 1997; J. Wang et al. 2022), underscoring the role of nonequilibrium chemistry in initiating the pathways toward oxalic acid formation.

$$CH_3OH \rightarrow CH_2OH + H \quad \Delta H_r^\circ(0\ K) = +395.9 \pm 0.3\ kJ\ mol^{-1} \tag{1}$$

$$CH_3OH \rightarrow CH_3O + H \quad \Delta H_r^\circ(0\ K) = +435.0 \pm 0.3\ kJ\ mol \tag{2}$$

Second, the suprathermal hydrogen atom can add to carbon dioxide to form the hydroxycarbonyl (HOCO) radical via reaction (3). This reaction is exoergic by 4.1 ± 0.4 kJ mol^{-1} (B. Ruscic & H. Bross 2026), with an entrance barrier of 106 kJ mol^{-1}, computed at the MRCISD+Q/cc-pVTZ//CASSCF/cc-pVTZ level of theory (X. Song et al. 2006). The formation of the hydroxycarbonyl radical in electron-irradiated carbon dioxide-bearing ices has been demonstrated in previous laboratory studies on electron-irradiated carbon dioxide-containing ices (N. F. Kleimeier et al. 2020; J. Wang et al. 2024a; J. H. Marks et al. 2025; J. Wang et al. 2025a). The barrier to addition can be overcome by the kinetic energy of the suprathermal hydrogen atoms. Moreover, at irradiation doses identical to those employed in the present study, previous experiments on electron-irradiated carbon dioxide–methanol ices suggested the formation of hydroxycarbonyl radicals, which subsequently recombined with hydroxymethyl and methoxy radicals to yield glycolic acid ($HOCH_2COOH$) and carbonic acid monomethyl ester (CH_3OCOOH), respectively (J. H. Marks et al. 2023a). Third, two neighboring hydroxycarbonyl radicals can undergo barrierless radical–radical recombination to form oxalic acid via reaction (4), provided that they adopt a favorable geometry (C. d. B. Olivares et al. 2024; A. M. Turner et al. 2026). This recombination is strongly exoergic, releasing 358.7 ± 1.3 kJ mol^{-1} (B. Ruscic & H. Bross 2026). Although hydroxycarbonyl radicals may recombine during irradiation when generated in favorable geometries, trapped hydroxycarbonyl radicals may also undergo recombination during TPD as their mobility increases. However, the present experiments cannot determine whether oxalic acid forms at 5 K during irradiation, during TPD, or through contributions from both processes. Recall that the TPD profile of $m/z = 92$ from the irradiated CO_2–CD_3OD ice matches that of $m/z = 90$ from the irradiated CO_2–CH_3OH ice, demonstrating the incorporation of two hydrogen atoms from methanol into oxalic acid. Because the relatively low irradiation dose employed here is expected to limit secondary production of hydroxycarbonyl radicals from methanol, the initially deposited carbon dioxide is considered the most plausible dominant carbon source for oxalic acid formation

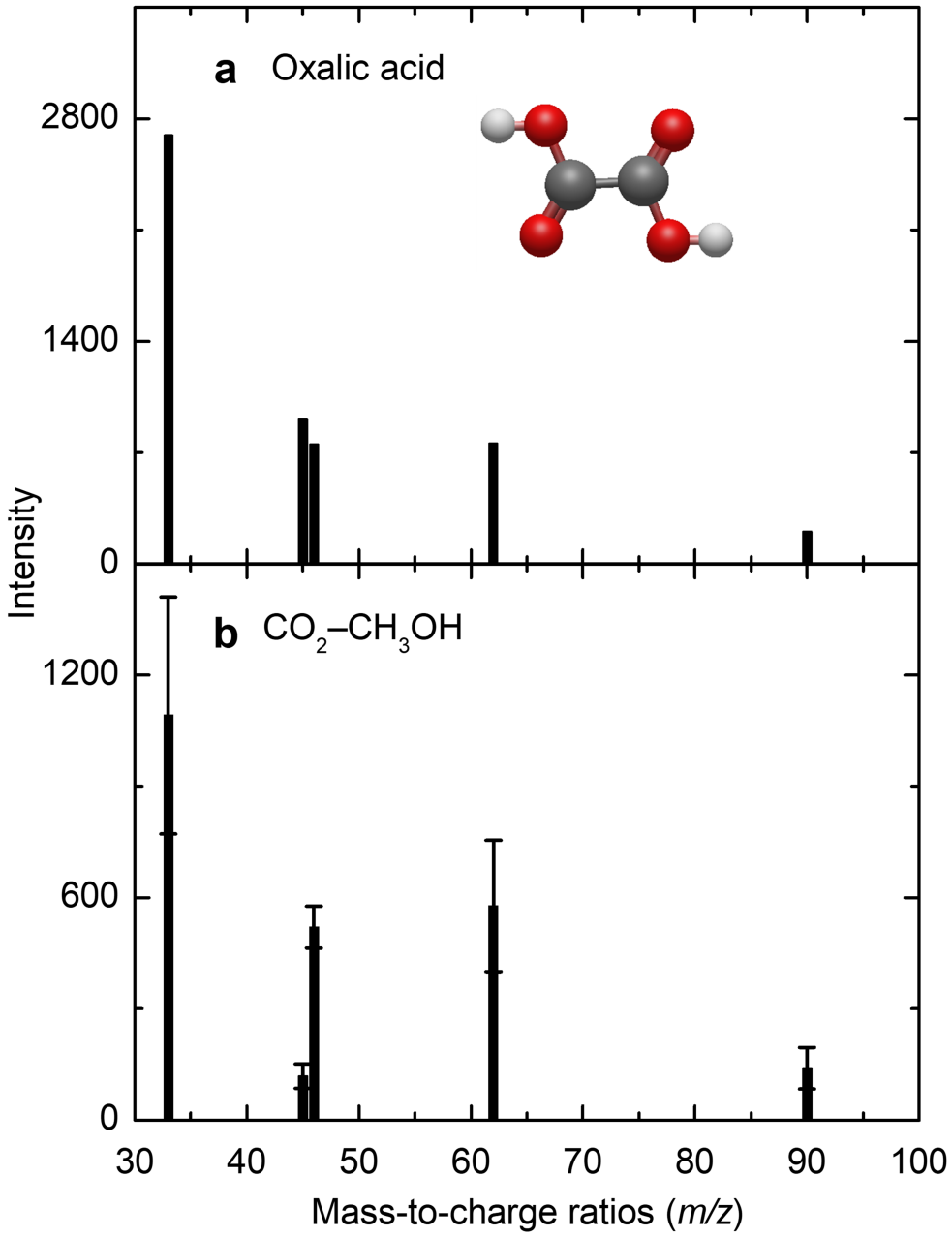

Figure 4. Integrated ion signals at distinct mass-to-charge ratios relevant to fragment and parent ions (HO_2^+, CHO_2^+, $CH_2O_2^+$, $CH_2O_3^+$ and $C_2H_2O_4^+$) of gas-phase oxalic acid at a photoionization energy of 11.10 eV, extracted from (a) the ReToF mass spectrum (R. Komorek et al. 2018), and (b) irradiated CO_2–CH_3OH ice.

under the present experimental conditions.

$$CO_2 + H \rightarrow HOCO \quad \Delta H_r^\circ(0\ K) = -4.1 \pm 0.4\ kJ\ mol^{-1} \tag{3}$$

$$HOCO + HOCO \rightarrow HOOCCOOH \quad \Delta H_r^\circ(0\ K) = -358.7 \pm 1.3\ kJ\ mol^{-1}. \tag{4}$$

4. Astrophysical Implications and Conclusions

This work presents the first laboratory simulation experiments demonstrating the abiotic formation of oxalic acid (HOOCCOOH) in interstellar ice analogs composed of carbon dioxide and methanol. The ices were exposed to energetic electrons as proxies for secondary electrons generated through the interaction of GCRs with interstellar ices in cold molecular clouds. The applied irradiation dose corresponds to $(7 \pm 1) \times 10^6$ yr of GCR exposure, representative of an evolved stage of a cold molecular cloud, whose lifetime may extend to 5×10^7 yr (A. G. Yeghikyan 2011). Oxalic acid was identified isomer-selectively in the gas phase by PI-ReToF-MS during TPD based on its IE and isotopic substitution experiments, with the assignment further supported by its dissociative photoionization fragmentation pattern. The TPD process simulates the thermal processing of interstellar ices as cold molecular clouds evolve toward star-forming regions. The formation of oxalic acid can proceed through the electron-induced generation of

suprathermal hydrogen atoms, their subsequent addition to carbon dioxide to form the hydroxycarbonyl radical, and the barrierless recombination of two hydroxycarbonyl radicals. These results reveal a feasible formation pathway for oxalic acid in carbon dioxide-bearing interstellar ices through GCR-driven processes and provide valuable constraints for astrochemical modeling of its abiotic synthesis and astrochemical evolution in extraterrestrial environments. Future studies should explore more realistic interstellar ice compositions, particularly water-rich mixtures, given that water is the most abundant constituent of interstellar ices.

Carbon dioxide is one of the most abundant constituents of interstellar ices, whereas methanol abundances vary considerably among different astrophysical environments (K. I. Öberg et al. 2011). Both carbon dioxide (CO_2) and methanol (CH_3OH) have been identified in ices by JWST toward the background stars NIR38 and J110621 in the Chamaeleon I molecular cloud (M. K. McClure et al. 2023). Both species are also present in ices associated with YSOs, including Class 0 protostars such as IRAS 15398−3359 (Y.-L. Yang et al. 2022), Ser-emb7, L483, and B335 (A. M. Turner et al. 2026), as well as massive embedded protostars such as W33A (E. L. Gibb et al. 2000) and RAFGL7009S (E. Dartois et al. 1999). The carbon dioxide–methanol ice employed here serves as a simplified model system to investigate low-temperature pathways leading to oxalic acid rather than reproduce the full complexity of interstellar ices, thereby providing a basis for future studies of more realistic ice mixtures. The formation of oxalic acid in electron-irradiated carbon dioxide–methanol ices demonstrated here therefore suggests that GCR-driven nonequilibrium chemistry may provide a viable pathway to its synthesis in environments where carbon dioxide and methanol-bearing ices coexist. The integrated ion signal of oxalic acid in the irradiated CO_2–CH_3OH ice recorded at 11.10 eV was 2446 ± 375 counts, including contributions from the parent and fragment ions, and was comparable in magnitude to those of carbonic acid monomethyl ester (CH_3OCOOH; 2342 ± 274 counts) and glycolic acid ($HOCH_2COOH$; 1568 ± 274 counts), previously identified in the CO_2–CH_3OH ice under the same irradiation dose (J. H. Marks et al. 2023a). The abundance of glycolic acid relative to molecular hydrogen (H_2) has an upper limit of 1.7×10^{-10} toward the G+0.693−0.027 molecular cloud (I. Jiménez-Serra et al. 2020); oxalic acid and glycolic acid yield comparable integrated ion signals under the present experimental conditions, suggesting an estimated upper abundance limit for oxalic acid of a few 10^{-10} relative to H_2. Future studies should investigate the formation of oxalic acid by incorporating major interstellar constituents such as water (H_2O), carbon monoxide (CO), or ammonia (NH_3) into the ice mixtures. In such ice mixtures, hydroxyl (OH) and amino (NH_2) radicals generated from H_2O and NH_3, respectively, together with formyl (HCO) radicals formed through hydrogenation of CO, may recombine with hydroxycarbonyl radicals to form carbonic acid (HOCOOH) (M. Sanz-Novo et al. 2023), carbamic acid (NH_2COOH) (J. H. Marks et al. 2023b), and glyoxylic acid (HCOCOOH) (A. K. Eckhardt et al. 2019), respectively. These competing pathways may reduce the availability of hydroxycarbonyl radicals and thereby decrease the formation efficiency of oxalic acid. Once formed in interstellar ices, oxalic acid could subsequently be released into the gas phase as molecular clouds evolve toward star-forming regions and icy grains undergo thermal processing. Although the trans–trans–trans conformer of oxalic acid, which represents the lowest energy conformer, has no permanent electric dipole moment (V. M. Rivilla et al. 2026), the rotational spectrum of the higher-energy cis–trans–trans conformer has been characterized by microwave spectroscopy, and the latter has a large dipole moment of 3.073 D (P. D. Godfrey et al. 2000). Therefore, although oxalic acid has not yet been detected in the ISM, its polar cis–trans–trans conformer represents a promising target for future astronomical searches using radio telescopes such as the Atacama Large Millimeter/submillimeter Array (ALMA), particularly toward the aforementioned sources.

Additionally, 28 products were predicted from the radical–radical recombination among the radicals generated from abundant interstellar ice constituents, including methane (CH_4), ammonia (NH_3), water (H_2O), methanol (CH_3OH), carbon dioxide (CO_2), and carbon monoxide (CO) (A. C. A. Boogert et al. 2015). A hydroxycarbonyl radical could react barrierlessly with hydrogen atoms, methyl (CH_3), amino (NH_2), hydroxyl (OH), hydroxymethyl (CH_2OH), methoxy (CH_3O), and formyl (HCO) radicals (A. M. Turner et al. 2026), leading to the formation of formic acid (HCOOH), acetic acid (CH_3COOH) (C. J. Bennett & R. I. Kaiser 2007), carbamic acid (NH_2COOH) (J. H. Marks et al. 2023b), carbonic acid (HOCOOH) (W. Zheng & R. I. Kaiser 2007), glycolic acid, carbonic acid monomethyl ester (J. H. Marks et al. 2023a), and glyoxylic acid (HCOCOOH) (A. K. Eckhardt et al. 2019), respectively (Figure 5). Notably, 27 of these species have been identified in our laboratory simulations of interstellar ice analogs, with methoxyamine (CH_3ONH_2) representing the only exception (Figure 5). Among these oxygen-containing products, three carboxylic acids—formic acid, acetic acid, and carbonic acid—have already been detected in interstellar environments. Formic acid was first detected toward the Galactic center molecular cloud Sagittarius B2 (Sgr B2) using the NRAO 140-foot radio telescope (B. Zuckerman et al. 1971; G. Winnewisser & E. Churchwell 1975). Acetic acid was subsequently detected and confirmed toward the Sgr B2 Large Molecule Heimat (LMH) source using the Berkeley–Illinois–Maryland Association (BIMA) Array and the Caltech Owens Valley Radio Observatory (OVRO) Millimeter Array (D. M. Mehringer et al. 1997). More recently, the cis–trans conformer of carbonic acid was identified toward the Galactic center molecular cloud G+0.693–0.027 using the Yebes 40 m and IRAM 30 m telescopes (M. Sanz-Novo et al. 2023). Acetic acid and cis–trans carbonic acid have been detected toward the G+0.693−0.027 molecular cloud with abundances relative to H_2 of $(3.1 \pm 0.2) \times 10^{-10}$ and $(4.7 \pm 0.3) \times 10^{-11}$, respectively (M. Sanz-Novo et al. 2023). Notably, both formic acid and acetic acid have been detected toward Sgr B2, where methanol is abundant and an enhanced abundance of carbon dioxide has been inferred toward the Sgr B2 envelope (J. L. Neill et al. 2014). These observations demonstrate the coexistence of carboxylic acids with carbon dioxide- and methanol-rich environments and, together with the present experimental results, motivate future searches for oxalic acid toward sources such as Sgr B2.

Lastly, oxalic acid could act as a precursor to more complex, potentially prebiotic oxygen-containing COMs through reactions with abundant constituents of interstellar ices under nonequilibrium conditions driven by UV photons or GCRs. Once formed, these compounds could be preserved during the gravitational collapse of molecular clouds, incorporated into circumstellar disks, and ultimately incorporated into primitive solar system bodies such as asteroids and comets

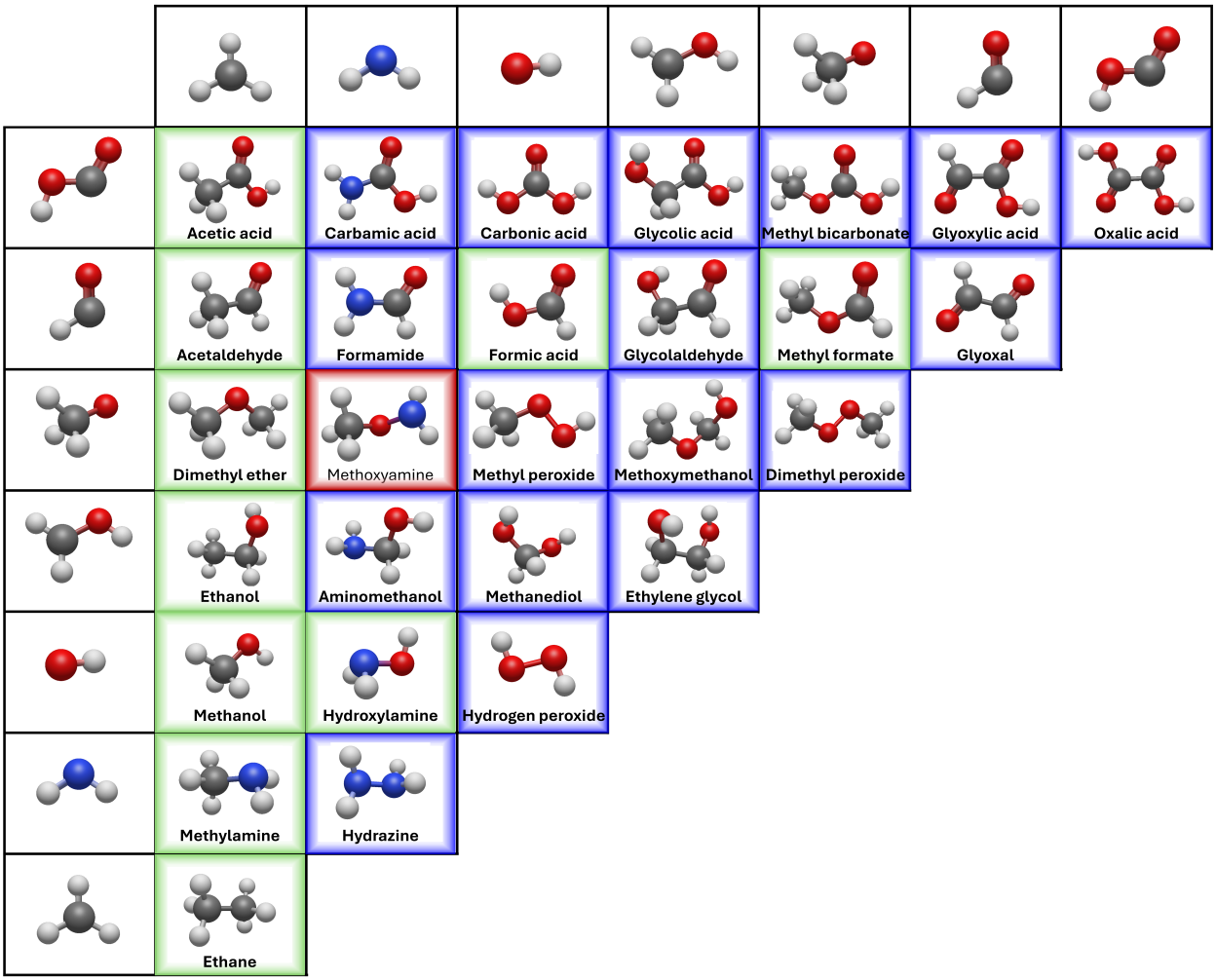

Figure 5. Products from barrierless radical–radical recombination reactions in ices adapted from Turner at al 2026 (A. M. Turner et al. 2026). Radical reactants are arranged along the left column and top row and include the hydroxycarbonyl (HOCO), formyl (HCO), methoxy (CH_3O), hydroxymethyl (CH_2OH), amino (NH_2), hydroxyl (OH), and methyl (CH_3) radicals. Products highlighted in green indicate molecules potentially observed by JWST in interstellar ices, whereas those in blue were not identified in ice spectra toward Class 0 protostars, but were detected in our laboratory simulation experiments; products in red were not detected by either method.

(A. K. Eckhardt et al. 2019; Y. Furukawa et al. 2019). Notably, pristine samples returned from asteroid Ryugu contain dicarboxylic acids including oxalic acid, along with monocarboxylic acids, hydroxy acids, and keto acids (Y. Takano et al. 2024). Moreover, a variety of dicarboxylic acids extending to C_9 species such as azelaic acid have been identified in carbonaceous chondrites, with oxalic acid reported as the most abundant dicarboxylic acid (E. T. Peltzer et al. 1984; A. Shimoyama & R. Shigematsu 1994). Following incorporation and subsequent chemical processing within primitive bodies, these compounds could ultimately have been delivered exogenously to the early Earth, providing molecular feedstocks for prebiotic chemical evolution and the synthesis of increasingly complex biorelevant molecules (H. G. Changela et al. 2024).

Acknowledgments

We acknowledge support from the U.S. National Science Foundation (NSF), Division of Astronomical Sciences under grant AST-2403867 awarded to R.I.K. at the University of Hawaii at Manoa. M.A. was supported by the Gas Phase Chemical Physics Program, in the Chemical Sciences, Geosciences, and Biosciences Division of the Office of Basic Energy Sciences of the U.S. Department of Energy under Contract No. DE-AC02-05CH11231.

Appendix

The FTIR spectra of CO_2−CH_3OH ices before and after electron irradiation are shown in Figure A1. The photoionization mass spectrum of gas-phase oxalic acid recorded at a photon energy of 11.10 eV is presented in Figure A2.

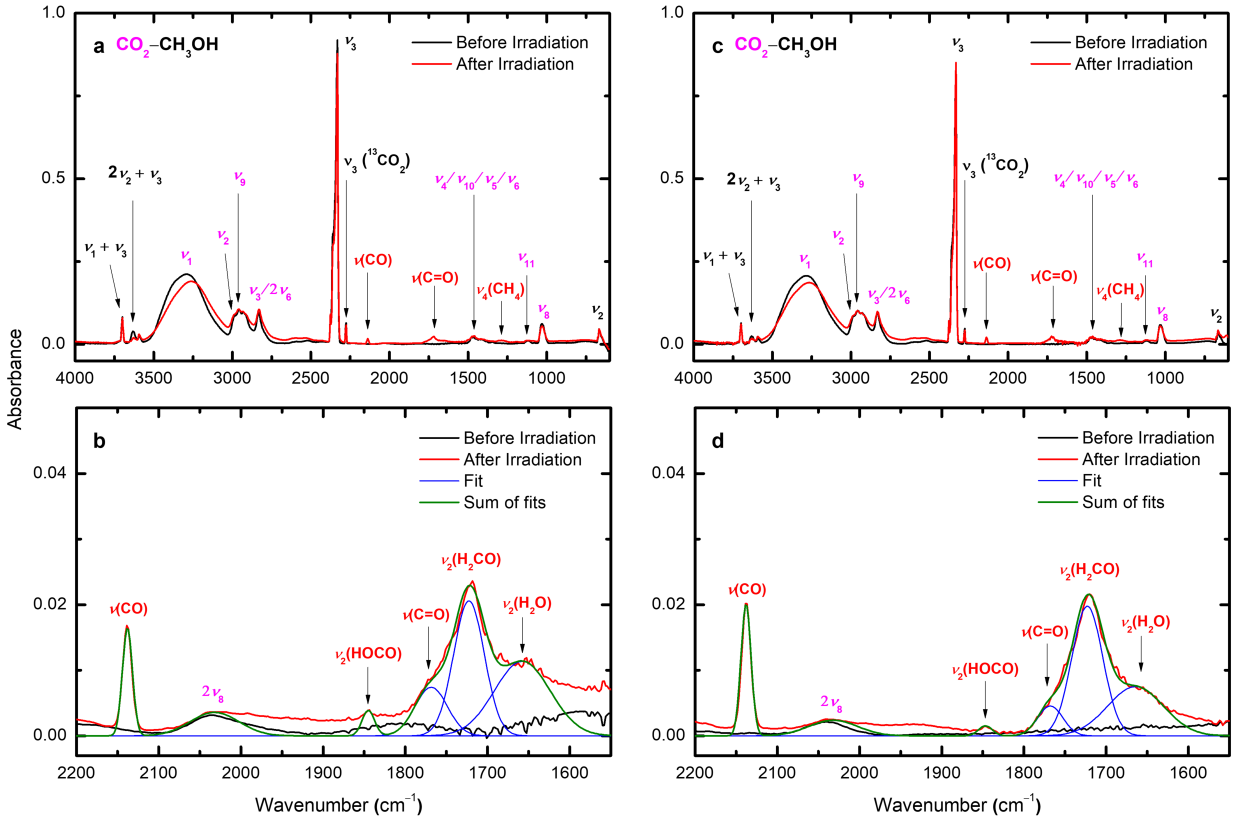

Figure A1. Baseline-corrected infrared spectra of CO_2−CH_3OH ices before and after electron irradiation at 5 K under low-dose (50 nA, 30 minutes; panels (a) and (b)) and higher-dose (100 nA, 60 minutes; panels (c) and (d)) conditions. Panels (b) and (d) show magnified views of the 2200–1550 cm^{-1} region after irradiation, together with Gaussian deconvolution of the absorption features. Atmospheric suppression was applied to the spectrum in (d). Absorptions assigned to CO_2, CH_3OH, and newly formed species are labeled in magenta, black, and red, respectively.

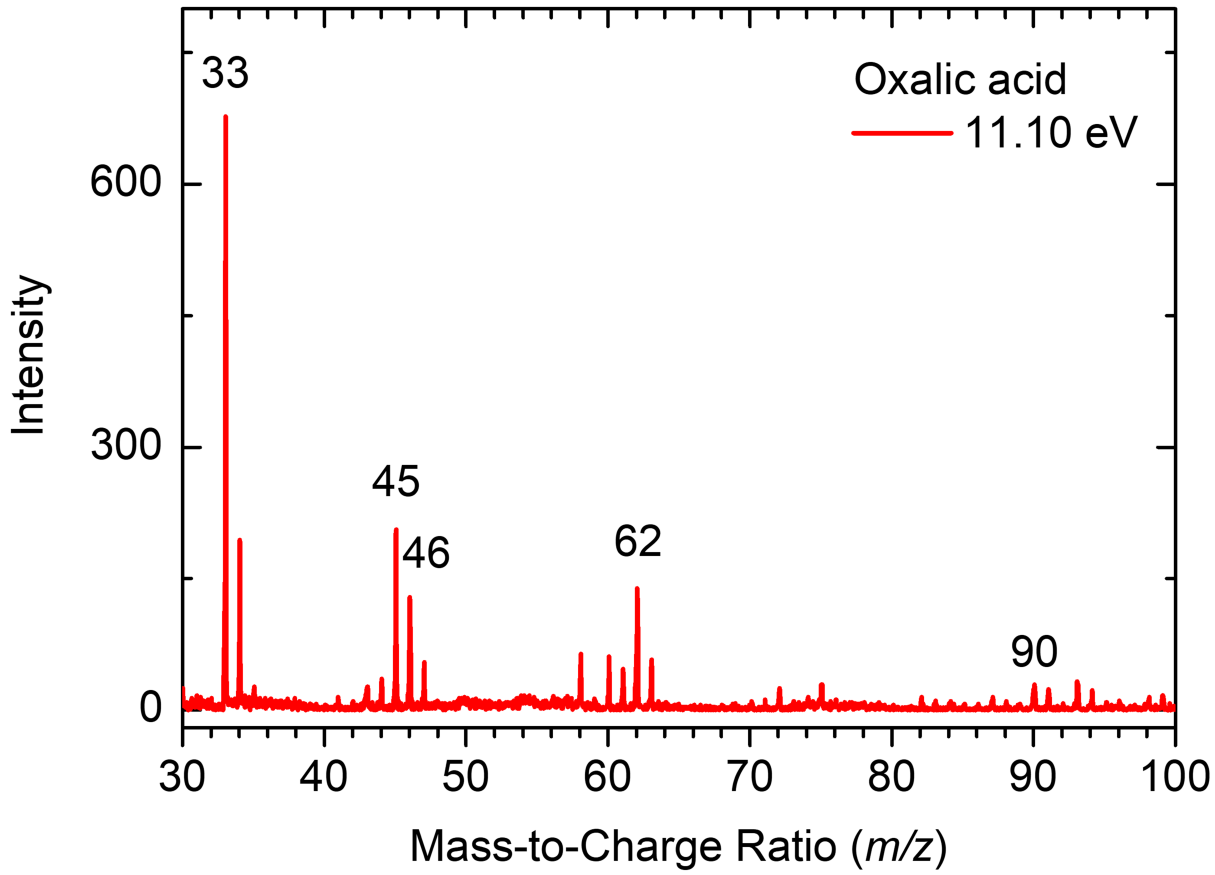

Figure A2. VUV photoionization mass spectrum of gas-phase oxalic acid recorded at a photon energy of 11.10 eV (R. Komorek et al. 2018).

ORCID iDs

Jia Wang https://orcid.org/0000-0002-3795-8699
Musahid Ahmed https://orcid.org/0000-0003-1216-673X
Ralf I. Kaiser https://orcid.org/0000-0002-7233-7206

References

Bennett, C. J., & Kaiser, R. I. 2007, ApJ, 660, 1289
Bergantini, A., Abplanalp, M. J., Pokhilko, P., et al. 2018a, ApJ, 860, 108
Bergantini, A., Góbi, S., Abplanalp, M. J., & Kaiser, R. I. 2018b, ApJ, 852, 70
Bergantini, A., Maksyutenko, P., & Kaiser, R. I. 2017, ApJ, 841, 96
Boogert, A. C. A., Gerakines, P. A., & Whittet, D. C. B. 2015, ARA&A, 53, 541
Bouilloud, M., Fray, N., Benilan, Y., et al. 2015, MNRAS, 451, 2145
Butscher, T., Duvernay, F., Danger, G., & Chiavassa, T. 2016, A&A, 593, A60
Cazaux, S., Tielens, A. G. G. M., Ceccarelli, C., et al. 2003, ApJ, 593, L51
Changela, H. G., Kebukawa, Y., Petera, L., et al. 2024, NatCo, 15, 6165
Cooper, G., Reed, C., Nguyen, D., Carter, M., & Wang, Y. 2011, PNAS, 108, 14015
Dartois, E., Schutte, W. A., Geballe, T. R., et al. 1999, A&A, 342, L32
De Villepin, J., Novak, A., & Bougeard, D. 1982, CP, 73, 291
Drouin, D., Couture, A. R., Joly, D., et al. 2007, Scanning, 29, 92
Eckhardt, A. K., Bergantini, A., Singh, S. K., Schreiner, P. R., & Kaiser, R. I. 2019, AngCh, 58, 5663
Fernández, I., & Frenking, G. 2007, JPCA, 111, 8028
Ferrari, B. C., Slavicinska, K., & Bennett, C. J. 2021, AcChR, 54, 1067
Furukawa, Y., Chikaraishi, Y., Ohkouchi, N., et al. 2019, PNAS, 116, 24440
Gibb, E. L., Whittet, D. C. B., Boogert, A. C. A., & Tielens, A. G. G. M. 2004, ApJS, 151, 35
Gibb, E. L., Whittet, D. C. B., Schutte, W. A., et al. 2000, ApJ, 536, 347
Godfrey, P. D., Mirabella, M. J., & Brown, R. D. 2000, JPCA, 104, 258
Herbst, E., & Dishoeck, E. F. V. 2009, ARA&A, 47, 427
Hudson, R. L., Loeffler, M. J., Ferrante, R. F., Gerakines, P. A., & Coleman, F. M. 2020, ApJ, 891, 22
Jiménez-Serra, I., Martín-Pintado, J., Rivilla, V. M., et al. 2020, AsBio, 20, 1048
Jones, B. M., & Kaiser, R. I. 2013, JPCL, 4, 1965
Kaiser, R., Eich, G., Gabrysch, A., & Roessler, K. 1997, ApJ, 484, 487
Kaiser, R., & Roessler, K. 1997, ApJ, 475, 144
Kaiser, R. I., Maity, S., & Jones, B. M. 2014, PCCP, 16, 3399
Kim, Y. S., & Kaiser, R. I. 2010, ApJ, 725, 1002
Kleimeier, N. F., Eckhardt, A. K., Schreiner, P. R., & Kaiser, R. I. 2020, Chem, 6, 3385
Komorek, R., Xu, B., Yao, J., et al. 2018, RScI, 89, 115105
Lawless, J. G., Zeitman, B., Pereira, W. E., Summons, R. E., & Duffield, A. M. 1974, Natur, 251, 40
Lerner, N. R., & Cooper, G. W. 2005, GeCoA, 69, 2901
Maity, S., Kaiser, R. I., & Jones, B. M. 2015, PCCP, 17, 3081
Marín-Yaseli, M. R., González-Toril, E., Mompeán, C., & Ruiz-Bermejo, M. 2016, CEJ, 22, 12785
Marks, J. H., Bai, X., Nikolayev, A. A., et al. 2025, NatCo, 16, 6468
Marks, J. H., Bai, X., Nikolayev, A. A., et al. 2024, JAChS, 146, 12174
Marks, J. H., Wang, J., Evseev, M. M., et al. 2023a, ApJ, 942, 43
Marks, J. H., Wang, J., Sun, B.-J., et al. 2023b, ACSCS, 9, 2241
Materese, C. K., Cruikshank, D. P., Sandford, S. A., Imanaka, H., & Nuevo, M. 2015, ApJ, 812, 150
Materese, C. K., Cruikshank, D. P., Sandford, S. A., et al. 2014, ApJ, 788, 111
Materese, C. K., Nuevo, M., Bera, P. P., Lee, T. J., & Sandford, S. A. 2013, AsBio, 13, 948
McClure, M. K., Rocha, W. R. M., Pontoppidan, K. M., et al. 2023, NatAs, 7, 431
McMurtry, B. M., Saito, S. E. J., Turner, A. M., Chakravarty, H. K., & Kaiser, R. I. 2016a, ApJ, 831, 174
McMurtry, B. M., Turner, A. M., Saito, S. E. J., & Kaiser, R. I. 2016b, CP, 472, 173

Mehringer, D. M., Snyder, L. E., Miao, Y., & Lovas, F. J. 1997, ApJL, 480, L71
Milligan, D. E., & Jacox, M. E. 1971, JChPh, 54, 927
Mukherjee, N., & Ghorai, U. K. 2025, ACS Catal, 15, 14823
Neill, J. L., Bergin, E. A., Lis, D. C., et al. 2014, ApJ, 789, 8
Nuevo, M., & Sandford, S. A. 2014, ApJ, 793, 125
Öberg, K. I., Boogert, A. A., Pontoppidan, K. M., et al. 2011, ApJ, 740, 109
Olivares, C. d B., Carrascosa, H., Escribano, B., Caro, G. M. M., & Martín-Doménech, R. 2024, MNRAS, 527, 8829
Parise, B., Ceccarelli, C., Tielens, A. G. G. M., et al. 2002, A&A, 393, L49
Peltzer, E. T., Bada, J. L., Schlesinger, G., & Miller, S. L. 1984, AdSpR, 4, 69
Pontoppidan, K. M., Boogert, A. C., Fraser, H. J., et al. 2008, ApJ, 678, 1005
Remusat, L., Derenne, S., & Robert, F. 2005, GeCoA, 69, 4377
Rivilla, V. M., Sanz-Novo, M., & San Andrés, D. 2026, ESC, 10, 1155
Ruscic, B., & Bross, H. 2026, Active Thermochemical Tables (ATcT) values based on ver. 1.220 of the Thermochemical Network (accessed 29 May, 2026), Argonne National Laboratory, https://atct.anl.gov/Thermochemical%20Data/version%201.220/index.php
Sanz-Novo, M., Rivilla, V. M., Jiménez-Serra, I., et al. 2023, ApJ, 954, 3
Schumann, D., Hartman, H., Eberl, D. D., et al. 2012, AsBio, 12, 549
Shimoyama, A., & Shigematsu, R. 1994, Chem Lett, 23, 523
Socrates, G. 2004, Infrared and Raman Characteristic Group Frequencies: Tables and Charts (3rd ed.; Wiley)
Song, X., Li, J., Hou, H., & Wang, B. 2006, JChPh, 125, 094301
Sturm, J. A., McClure, M. K., Beck, T. L., et al. 2023, A&A, 679, A138
Takano, Y., Naraoka, H., Dworkin, J. P., et al. 2024, NatCo, 15, 5708
Turner, A. M., Abplanalp, M. J., Chen, S. Y., et al. 2015, PCCP, 17, 27281
Turner, A. M., & Kaiser, R. I. 2020, AcChR, 53, 2791
Turner, A. M., Yang, Y.-L., Gross, R., Sakai, N., & Kaiser, R. I. 2026, ApJ, 1000, 17
Wang, J., Marks, J. H., Fortenberry, R. C., & Kaiser, R. I. 2024a, SciA, 10, eadl3236
Wang, J., Marks, J. H., Tuli, L. B., et al. 2022, JPCA, 126, 9699
Wang, J., Marks, J. H., Turner, A. M., et al. 2023a, PCCP, 25, 936
Wang, J., Nikolayev, A. A., Marks, J. H., et al. 2023b, JPCL, 14, 6078
Wang, J., Turner, A. M., Marks, J. H., Fortenberry, R. C., & Kaiser, R. I. 2024b, ChPhC, 25, e202400837
Wang, J., Zhang, C., Bergantini, A., et al. 2025a, JAChS, 147, 29088
Wang, J., Zhang, C., Eckhardt, A. K., & Kaiser, R. I. 2025b, Chem Sci, 16, 21111
Wang, J., Zhang, C., Marks, J. H., et al. 2024c, NatCo, 15, 10189
Whittet, D. C. B., Gerakines, P. A., Tielens, A. G. G. M., et al. 1998, ApJ, 498, L159
Winnewisser, G., & Churchwell, E. 1975, ApJ, 200, L33
Xie, M., Matsuda, Y., & Fujii, A. 2015, JPCA, 119, 5668
Yan, H., & Chu, L. T. 2008, Langm, 24, 9410
Yang, Y.-L., Green, J. D., Pontoppidan, K. M., et al. 2022, ApJL, 941, L13
Yeghikyan, A. G. 2011, Ap, 54, 87
Zheng, W., & Kaiser, R. I. 2007, CPL, 450, 55
Zhu, C., Frigge, R., Bergantini, A., Fortenberry, R. C., & Kaiser, R. I. 2019, ApJ, 881, 156
Zuckerman, B., Ball, J. A., & Gottlieb, C. A. 1971, ApJ, 163, L41